RSC Advances

ROYAL SOCIETY OF CHEMISTRY

www.rsc.org/advances

Ultra-thin C_3N_4 nanosheet as the rapid charge transfer in a core-shell heterojunction of α-sulfur@C_3N_4 for super metal-free photocatalysis under visible light

Xueming Dang, Xiufang Zhang*, Weiqiang Zhang, Xiaoli Dong, Guowen Wang, Chun Ma, Xinxin Zhang, Hongchao Ma, Mang Xue

School of Light Industry and Chemical Engineering, Dalian Polytechnic University, Dalian, China, 116034

Corresponding Author

Tel.: +86 411 86323508; fax: +86 411 86323736. E-mail address: zhangxf@dlpu.edu.cn.

Abstract The core-shell heterojunctions of ultra-thin C_3N_4 nanosheet enwrapped spherical α-S (α-S@C_3N_4) were fabricated via self-assemble process by electrostatic force to enhance its photocatalytic ability under visible light. The photocatalytic ability can be adjusted by tuning the amount of the ultra-thin C_3N_4 nanosheet. α-S@C_3N_4 composite with 35% of the amount of C_3N_4 nanosheet has the highest photocatalytic ability. The degradation rate of Rhodamine B (RhB) with α-S@C_3N_4 (35% C_3N_4) is 6.72 times faster compared to α-S as photocatalyst. This increase could be attributed to the efficient photogenerated holes and electrons separation by the heterojunction, which has excellent charge transfer ability, arose by ultra-thin C_3N_4 nanosheet. The stability of the α-S is also largely improved by the heterojunction construction.

Keywords heterojunction, α-S, C_3N_4 nanosheet, visible light, photocatalysis

1. Introduction

Recently, more attention has been paid to the semiconductor photocatalysis in the field of pollution elimination as a "green" technology that can completely mineralizing most type of pollutants under the illumination of sunlight and moderate ambient conditions. [1-3] Development of an efficient visible-light-driven semiconductor material is a key need for practical application of this technology. With unique advantages of low cost, abundance, and easy access, the metal-free elemental photocatalysts are emerging and have great potential to be applied in practical industry. [4-6] Most recently, Liu et al. proved α-sulfur (α-S) as a candidate for visible-light-driven photocatalyst because of its capability of degrading Rhodamine B (RhB) under visible light illumination. [7] Then, in order to enhance the photocatalytic ability of α-S, some works have been done. Yu and co-workers [8] constructed heterojunction of graphene and g-C_3N_4 cowrapped α-S, and the enhanced photocatalytic ability of bacterial inactivation was found. Peng et al. [9] reported that sulfur/graphene composite was fabricated and the incorporation of graphene enhanced photocatalytic activity for the degradation of the methyl orange due to the increased hydrophilicity and adsorption capacity. However, similar as the other photocatalysts, α-S still has low quantum efficiency attributing from the limited light absorption ability, the high recombination rate of photogenerated holes and electrons, and the sluggish surface reaction.

It is well known that the photocatalytic activity is closely related to photocatalyst size, morphology, structure, and surface area etc. [10] Decrease of the size can enhance the photocatalytic activity due to increasing surface area exposed to the light and reactants. As a result, the light absorption and the surface reaction can be improved. Several surfactants have been used as the soft template in the fabrication of the photocatalysts for the size and

morphology control. [11] One example is Poly (vinyl pyrrolidone) (PVP), which has been proved to be an efficient template either to decrease the size or to configure the shape of the sphere. [12]

Fabrication of the heterojunction is another strategy for improving the photocatalytic activity potentially attributed from the highly effective charge separation. [13] When design a heterojunction, the critical factor that should be considered is the charge transportation ability of the loading material. One good example is Graphene, which is widely used for the construction of the heterojunction due to its extremely high electron mobility. [14] Recently, it was reported that bulk g-C_3N_4 can degrade organic pollutant under visible light irradiation. [15-17] It is a layered material, and can be exfoliated into ultra-thin nanosheet with a few layers, even into single atomic layer nanosheet. [18, 19] The exfoliated C_3N_4 nanosheet has big surface area with very thin layer thickness, and excellent conductivity with less resistant between layers, which make it an excellent material constructing heterojunctions with other semiconductors. Furthermore, the interface area of the heterojunction is a key parameter that can affect the photocatalytic ability. [20] The large contact area can promote the charge transfer across the interface, thereby increase the separation of electron-hole pairs, and lead to the enhancement of photocatalytic ability. Ideally, the approach to enhance photocatalytic ability is to increase the interface area of semiconductors of the heterojunction. Therefore, enwrap the spherical α-S with selected ultra-thin C_3N_4 nanosheet to obtain large contact area and thus improve catalyst efficiency based on this hypothesis. Another consideration when fabricating efficient heterojunction is the matching band potential of the semiconductors (denoted by semiconductor 1 and semiconductor 2). When the conduction band (CB) and valence band (VB) potential of semiconductor 1 are lower than those of semiconductor 2, respectively, the gradient of the potential level drives photogenerated electrons in the CB of semiconductor 2 to that of semiconductor 1, and photogenerated holes in

the VB of semiconductor 1 to that of semiconductor 2. Therefore, the electrons and holes are further separated and stored in different semiconductors, and the recombination of them can be suppressed. It is reported that the VB of α-S is 0.25 eV higher than that of anatase TiO_2. [7] The band gap of α-S is 2.79 eV. Therefore, the calculated CB and VB of α-S are -0.40 and 2.39 eV vs. NHE, respectively. The CB and VB level of g-C_3N_4 are -1.3 and 1.4 V vs NHE, respectively. [21] Considering the match of the CB and VB levels with those of α-S, ultra-thin C_3N_4 is suited to fabricate heterojunction with α-S.

In this study, the core-shell heterojunctions of ultra-thin C_3N_4 nanosheet enwrapped spherical α-S (α-S@C_3N_4) was firstly fabricated for enhanced photocatalytic ability under visible light illumination. Ultra-thin C_3N_4 nanosheet is firstly used as the efficient charge transporter in the heterojunction structure. Based on rapid charge transfer, big contact surface area and the matching VB and CB level of the two semiconductors, the enhanced photocatalytic ability is expected. RhB, a common pollutant in the industry wastewater, is selected as a test substance to evaluate the photocatalytic performance of as prepared samples.

2. Experimental section

Sample preparation

Preparation of hollow spherical α-S

Spherical α-S was fabricated by soft template process with PVP as the template. First, 1.5 g of $Na_2S_2O_3 \cdot 2H_2O$ was dissolved in 250 mL water at about 50 ℃, this solution was marked as solution A. In the meanwhile, 200 mg of PVP was dissolved in 25 mL of $C_2H_5OH/CH_3COOH/H_2O$ mixture (volume ratio of 1 : 1 : 3) by vigorous stirring, and the resulting PVP solution was noted as solution B. As the following step, solution B was added in solution A followed by stirring for 5 minutes. The resulting mixture was heated to 70 ℃

followed by addition of 12 mL of concentrated hydrochloric acid. The temperature was then maintained at 70 ℃ for 5 min with magnetic stirring. The products were collected by filtration and washed with distilled water until the pH reached 7. The collected samples were then dried at 60 ℃ for 2 h.

Preparation of ultra-thin C_3N_4 nanosheets

The ultra-thin C_3N_4 nanosheet was fabricated by a "bulk-nanosheet-ultra-thin nanosheet" route and the detail procedure was described elsewhere [19]. Briefly, the bulk g-C_3N_4 was milled into powder in a mortar, and transferred to a ceramic boat followed an annealing process at 550 ℃ for 200 mins (5 ℃ /min of heating rate). After annealing, a light yellow powder of C_3N_4 nanosheet was produced. Following that, 100 mg C_3N_4 nanosheet powder was dispersed in 100 mL methanol at room temperature and exfoliated by ultrasonic process for 4 h. The final product (ultra-thin nanosheet) was centrifuged and dried in vacuum at 50 ℃ for 6 h.

Preparation of core-shell heterojunctions of α-S@C_3N_4 composites

The spherical α-S was enwrapped by ultra-thin C_3N_4 nanosheet via self-assemble process by electrostatic force. The schematic procedure for preparing the core-shell heterojunctions of α-S@C_3N_4 is presented in Scheme 1. The ultra-thin C_3N_4 nanosheets were post functionalized in HCl (0.5 mol/L) for 1 h protonation to get a well-dispersed aqueous solution (1 mg/mL) prior to use. [22] The ultra-thin C_3N_4 nanosheet solution was then added drop wise into the spherical α-S suspension with negative charges under vigorous stirring. After 15 min, the products were collected by filtration and washed with distilled water until the pH reached 7. The samples were obtained by drying at 60 ℃ for 2 h. The samples with 25%，35% and 45% of mass rate of ultra-thin C_3N_4 nanosheets to α-S were named as S_1, S_2, and S_3, respectively.

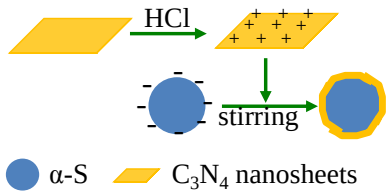

Scheme 1. Schematic procedure for preparing the core-shell heterojunctions of α-S@C_3N_4.

Sample characterization

The thickness and the morphology of C_3N_4 nanosheets were measured by an atomic force microscopy (AFM Agilent Pico Plus) and a transmission electron microscopy (TEM; JEM-2100(UHR) JEOL). X-ray diffraction (XRD) spectra were recorded by Rigaku D/MAX-2400 with Cu Ka radiation, accelerating voltage of 40 kV, current of 30 mA. The scanning rate was 8 ° (2θ)/min, and the scanning range was 10-80 °. Light absorption intensities were measured using a UV-vis spectrophotometer (Shimadzu, UV-2450) with a wavelength range of 200-800 nm. The morphology of the heterojunction composites was obtained by field emission scanning electron microscopy (FE-SEM, Hitachi S-4800) equipped with energy dispersive spectrometer (EDS) using the voltage of 5 kV, and the structure of heterojunction composites was characterized with high applied voltage of 15 kV and the EDS. Fluorescence (FL) spectra were recorded by FL spectrometer (LS-55, PE). The specific surface area was determined by an adsorption instrument (Tristar 3000) and calculated using the linear portion of the Brunauer-Emmett-Teller (BET) model.

Measurement of photocatalytic activity

The photocatalytic activities of the photocatalyst products were monitored through the degradation of RhB under visible light irradiation. Photocatalytic reactions were conducted in a 100 mL cuboid quartz reactor. A 300 W Xe lamp was used as visible light source. The light was

passed through a filter to shield any wavelength below 400 nm. The used light intensity was 30 mW/cm^2. In all experiments, 0.08 g of the photocatalyst was added in 80 mL RhB aqueous solution at 5mg/L. During each photocatalytic experiment, 5 mL of the suspension was collected at predetermined time intervals. The suspension was centrifuged at 9500 rpm for 10 min, and the concentration of RhB was determined by measuring the absorbance at λ=554 nm with a Shimadzu UV2000 spectrophotometer. The used photocatalyst was separated from the suspension, washed with deionized water and ethanol for three times, and then, dried at 60 ℃ for 6 h for the next experimental run.

3. Results and discussion

Analyses of C_3N_4 nanosheet characterization

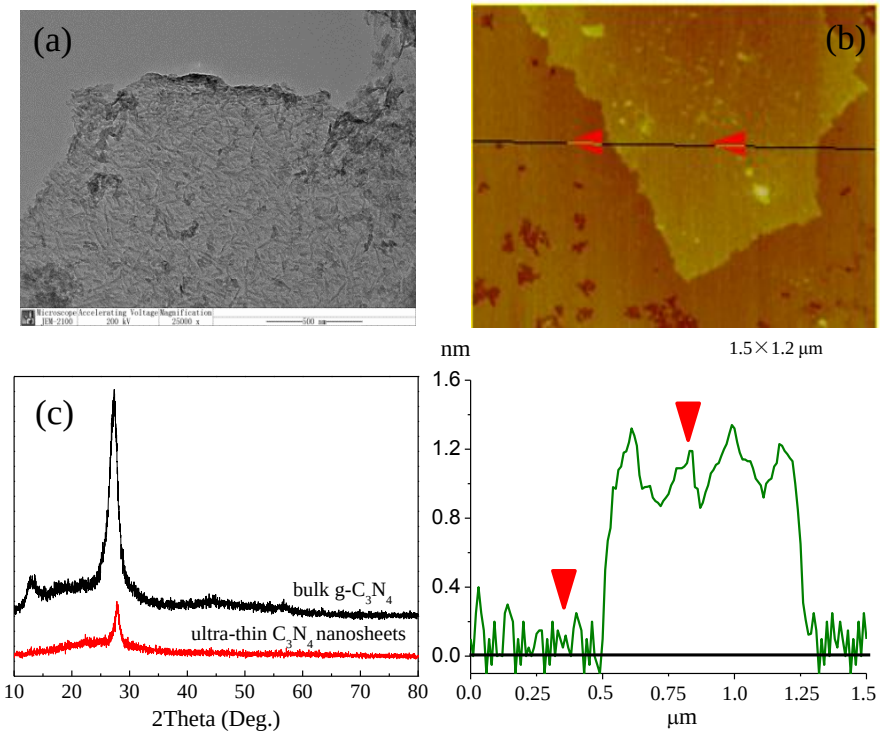

Figure 1 (a) TEM, (b) AMF image and (c) XRD pattern of the C_3N_4 nanosheet.

The collective analyses indicated ultra-thin C_3N_4 nanosheets have been obtained by exfoliation. The TEM image illustrates the very transparent feature of the C_3N_4 nanosheets (Figure 1 (a)), indicating the ultra-thin thickness of the nanosheets. The thickness of the nanosheets is 0.8-1.2 nm determined by the analysis of AFM image (Figure 1 (b)). Because the theoretical distance between each layer for the bulk g-C_3N_4 is 0.326 nm, [23, 24] it is assumed that two or three layers of ultra-thin C_3N_4 nanosheet is successfully fabricated. The XRD patterns are recorded and showed in Figure 1 (c). In the XRD pattern of bulk g-C_3N_4, the (002) diffraction at around 27.5° relates to the characteristic interlayer stacking structure, while the (100) diffraction at 13.1° indicates the interplanar structural packing. In the pattern of ultra-thin C_3N_4 nanosheet, the (002) diffraction related to the interlayer stacking is also found. However, the intensity is significantly less after exfoliation. This further demonstrated that the thickness of the C_3N_4 has been largely decreased.

Analyses of α-S@C_3N_4 heterojunction characterization

XRD analyses

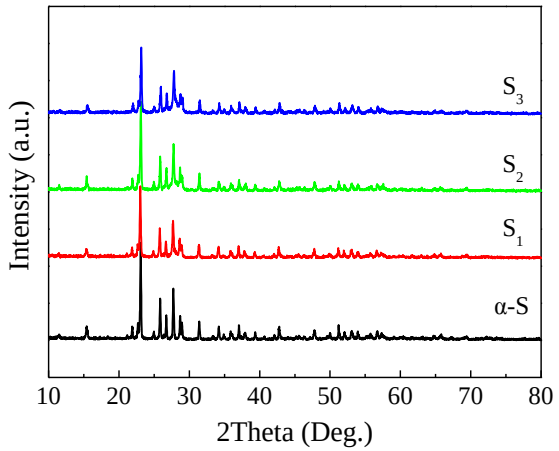

Figure 2 XRD patterns of the α-S, S_1, S_2 and S_3.

XRD patterns of the α-S, S_1, S_2 and S_3 are shown in Figure 2. Clear characteristic peaks with 2θ at 23.1°, 25.9°, 26.7°, 27.6°, 29.0° and 31.4° are observed in the pattern of α-S. The crystal form of α-S is orthorhombic structure, which is indexed to the standard cards (PDF No.77-0145).

The patterns of S_1, S_2 and S_3 are similar to that of α-S, indicating that the α-S in heterojunction composites is also orthorhombic structure, and fabrication of heterojuntions cannot change the crystal form of α-S. No diffraction peaks of ultra-thin C_3N_4 nanosheet are observed over the composite samples, which may be hidden by the spectral line of α-S.

Morphologies

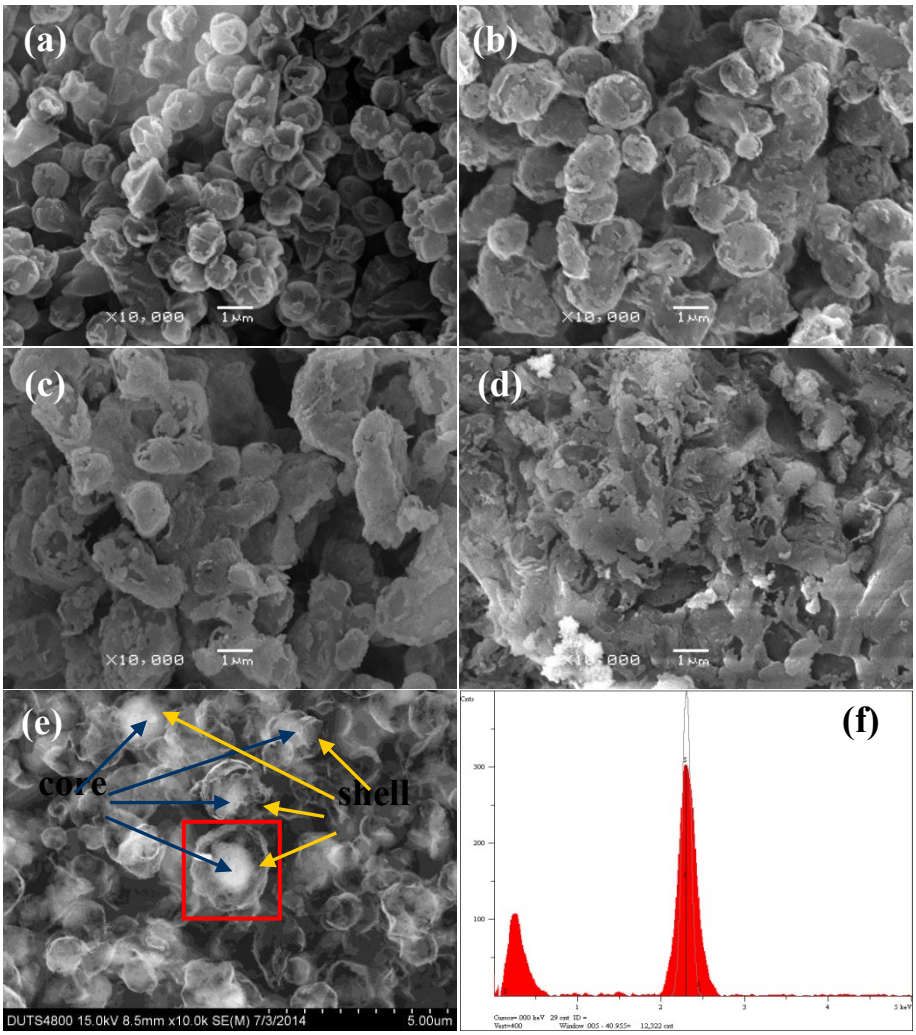

Figure 3 SEM images of (a) α-S, (b) S_1, (c) S_2, (d) S_3 and (e) SEM image of S_1 with high detection voltage (15 eV) and (f) EDS spectra of the rectangle of image (e).

The morphology of α-S is sphere with approximate 1 μm of the size (Figure 3 (a)). From the Figure 3(b) and (c), the particle is almost spherical shape. With the increase amount of ultra-thin

C_3N_4 nanosheets loaded, the size of the particle becomes larger, inferring that the C_3N_4 nanosheets have been loaded on α-S sphere and the thickness of loaded layer of C_3N_4 nanosheets become larger. However, when 45% C_3N_4 nanosheet was added in the composite, the original morphology of α-S disappears (Figure 3 (d)). Some of C_3N_4 nanosheets cannot be enwrapped on the α-S particles, and exist randomly in the composite. To further verify that some C_3N_4 nanosheets have been successfully enwrapped on the α-S sphere, the particle structure of S_1 is characterized by SEM with high detection voltage combined with the element detection with EDS. It is shown that the particles are constructed by two layers (Figure 3 (e)). And the particles are composed of C, N and S elements from the EDS analysis (Figure 3 (f)), demonstrating that ultra-thin C_3N_4 nanosheets have been enwrapped on the α-S sphere.

Optical absorption

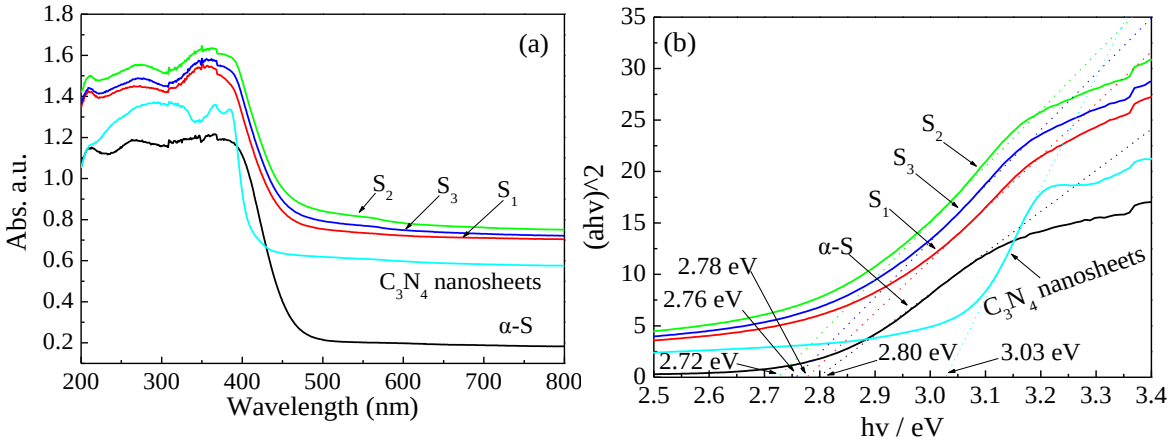

Figure 4 (a) UV-vis absorption spectra and (b) calculation of the band gap by Kubelka-Munk function of the α-S, C_3N_4 nanosheets, S_1, S_2 and S_3.

The optical absorption of the as-prepared samples was investigated using a UV-vis spectrometer. From Figure 4 (a), α-S shows intense absorption from 200 to 450 nm, indicating its visible-light-induced photocatalyst. The band gap is determined by the following formula:

$$\alpha h\nu = A(h\nu - E_g)^{n/2} \quad (1)$$

The calculated band gap is 2.80 eV (Figure 4 (b)), similar as previously reported value. The ultra-thin C_3N_4 nanosheet can absorb the light from 200 to about 410 nm. Its exact band gap is 3.03 eV, which is obviously smaller than that of bulk g-C_3N_4 (2.70 eV). This similar increase of the band gap has been reported previously, and is presumably attributed to the decrease of conjugation length and the strong quantum confinement effect from the ultra-thin structure of the prepared C_3N_4 nanosheets. [18, 25] The increased band gap of the ultra-thin C_3N_4 nanosheet is probably due to the negative shift of CB and/or the positive shift of VB. The VB and CB potential of ultra-thin C_3N_4 nanosheets are estimated based on the band gap difference (0.43 eV) of the ultra-thin C_3N_4 nanosheet and bulk g-C_3N_4 and the VB and CB level of bulk g-C_3N_4. The VB potential is between 1.4 and 1.83 eV, and the CB potential is between -1.73 and -1.3 eV. The calculated band gap of S_1, S_2 and S_3 are 2.78, 2.72 and 2.76 eV, respectively (shown in Figure 4(b)). Compared to α-S (2.8 eV), the decreases of the band gap are very minimum and can be ignored.

Separation ability of photogenerated charge carriers

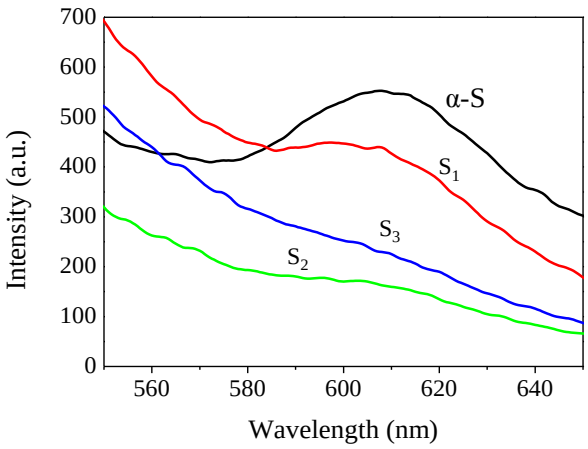

Figure 5 PL spectra of α-S, S_1, S_2 and S_3.

PL spectra analysis is used to reveal the separation efficiency of the photogenerated electrons and holes in semiconductors. Figure 5 is the PL spectra of S_1, S_2 and S_3 together with that of α-S for comparison. Considering that the PL emission results from the free charge carrier recombination, the lower peak indicates lower recombination rate of them. Compared to α-S, all three heterojunction composites show significant quenching of the PL, which suggests the separation of photogenerated electrons and holes can be improved by the construction of heterojuncitons between α-S and ultra-thin C_3N_4 nanosheets. The gradient of VB and CB of α-S and C_3N_4 drives the holes generated in α-S to the C_3N_4 nanosheet and the electrons generated in C_3N_4 nanosheet to α-S. Due to the excellent charge transfer ability of ultra-thin C_3N_4 nanosheet, the separated holes in ultra-thin C_3N_4 nanosheet are rapidly transferred to the reaction site, and then participate in the surface reaction. This rapid transportation further promotes the separation of photogeneated carrier pairs. Thus, the holes and electrons recombination can be largely suppressed.

The PL intensities of S_1, S_2 and S_3 are different. The intensity of S_2 is similar to that of S_3, which is lower than that of S_1. For the perspective of separation ability of photogenerated carriers, there is an optimal thickness of the coating layer in the heterojunction. [26] Compared to S_1, the C_3N_4 nanosheets layer of S_2 is thicker but still within the optimal thickness. Thus, the separation ability of photogenerated holes and electrons of S_1 is lower than that of S_2. Too many C_3N_4 nanosheets loaded increase the thickness of the C_3N_4 nanosheet layer, which is thicker than the optimal thickness. Thus, the separation efficiency of the electrons and holes is not enhanced.

Photocatalytic activity and stability

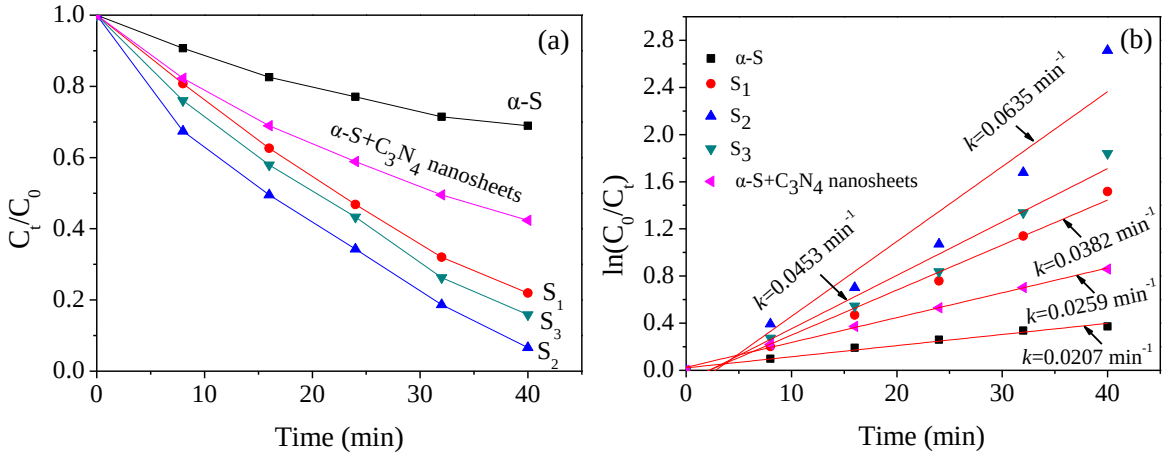

Figure 6 (a) C_t/C_0 and (b) $\ln(C_0/C_t)$ of the RhB concentration versus reaction time in photocatalytic degradation with α-S, S_1, S_2, S_3 and α-S and ultra-thin C_3N_4 nanosheet under visible light illumination.

Figure 6 (a) shows the photocatalytic activities of the α-S@C_3N_4 composites together with α-S for comparison. RhB concentration gradually decreases in the presence of α-S under visible light, and only 31.1% of RhB is removed after 40 min. However, at the same reaction condition, the removal rates of RhB with S_1, S_2 and S_3 are 78.1%, 93.4% and 84.1%, respectively. To quantitatively investigate the reaction kinetics of the RhB degradation, the experimental data are fitted by applying a first-order model as expressed by Eq. (1). This equation is well established for photocatalytic experiments when the pollutant is within the millimolar concentration range.

$$\ln(C_0/C_t) = kt \quad (1)$$

where C_0 and C_t are the dye concentrations at 0 and t of time, respectively, and k is the apparent first-order rate constant. In Figure 6 (b), the calculated k values of S_1, S_2 and S_3 are 0.0382, 0.0635 and 0.0453 min^{-1}, which are higher than that of α-S (0.00945 min^{-1}), demonstrating that heterojunction structure formed by enwrapping ultra-thin C_3N_4 nanosheet can enhance the photocatalytic ability of α-S. The k value of the S_2 is 6.72 times higher than that of α-S. This enhancement can be attributed to the separation efficiency of photogenerated holes and electrons. C_3N_4 nanosheet itself is also a visible-light-driven photocatalyst. To confirm the

heterojunction effect, the same amounts of ultra-thin C_3N_4 nanosheet (28 mg) and α-S (52 mg) to those of S_2 are used as the photocatalyst. Under the same condition, the RhB removal rate is largely lower than S_2, confirming that the enhanced photocatalytic ability of S_2 is attributed the heterojunction effect. The photocatalytic ability of ultra-thin C_3N_4 nanosheet is also determined (Fig. S1). The RhB removal rate is also lower than S_2, which can further confirm the heterojunction effect. The specific surface areas of α-S and α-S@C_3N_4 heterojunctions are also determined (See the supporting information). And the exact causal relationship of the specific surface area and the photocatalytic ability will be discussed in the following research.

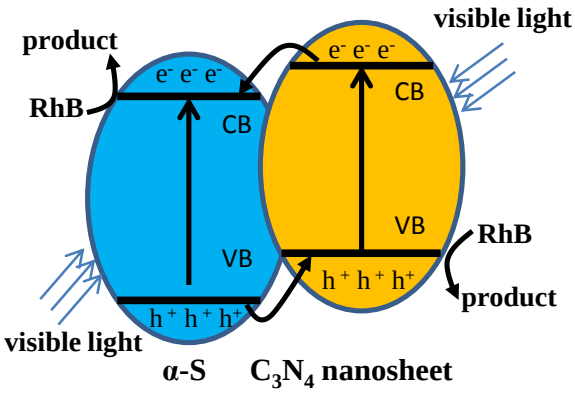

Figure 7 Proposed mechanism of enhanced photocatalytic ability of α-S@C_3N_4.

The possible mechanisms of enhanced photocatalytic ability of α-S@C_3N_4 under visible light illumination are proposed (Figure 7). Once illuminated by the visible light, α-S and ultra-thin C_3N_4 nanosheet are excited. Because the CB (between -1.73 and -1.3 eV vs. NHE) of ultra-thin C_3N_4 nanosheet is more negative than α-S, the photogenerated electrons in the CB of C_3N_4 nanosheet are injected to the CB of α-S. At the same time, the holes generated by α-S transport to the VB of C_3N_4 nanosheet due to the positive potential of α-S to ultra-thin C_3N_4 nanosheet (between 1.4 and 1.83 eV vs. NHE). The match of the CB and VB potential between two semiconductors makes the electrons and holes to remain separated. Therefore, the recombination

of electron-hole pairs is restrained and more electrons and holes can transfer to the surface of the composite and join in the surface reaction. So, the photocatalytic activity can be enhanced. The oxidizing species in the photocatalytic degradation of RhB with α-S and α-S@C_3N_4 are also probed (Figure S2). Compared with α-S, the heterojunction construction change the photocatalytic degradation pathway of RhB. ·OH radicals no longer serve as oxidizing species with α-S@C_3N_4 as catalyst, only holes and $\cdot O_2^-$ radicals contribute to the degradation of RhB. The data and detailed discussion can refer to the supporting information.

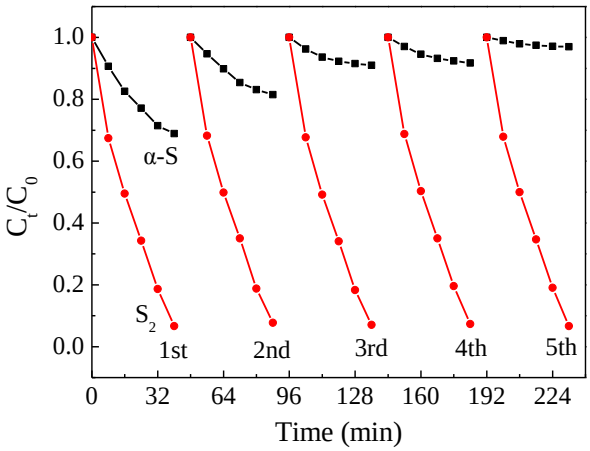

Figure 8 Cycling runs in the photocatalytic degradation of RhB with α-S and S_2 under visible light illumination.

The stability is one of the key parameters to evaluate the performance for a photocatalyst. Figure 8 shows the cycling performance of α-S and S_2 for degrading RhB in photocatalytic process under visible light illumination. After recycling and reusing for each cycle, the removal rate of α-S dramatically decreases from 31.1% of 1st cycle to 3.0% of 5^{th} cycle, indicating that α-S is aging in the photocatalytic process. In contrast, the removal rate of S_2 does not decrease obviously, inferring that coating C_3N_4 nanosheets on α-S can largely enhance the stability of α-S.

Based on the results listed above, α-S@C_3N_4 heterojuncion composite is proved to be a good candidate photocatalyst as efficient, recyclable and stable.

4. Conclusions

The core-shell heterojunctions of α-S@C_3N_4 are successfully fabricated via self-assemble process by electrostatic force. The enhancement of photocatalytic ability of α-S@C_3N_4 composite could be attributed to the efficient photogenerated holes and electrons separation by the heterojunction, which has excellent charge transfer ability arisen by ultra-thin C_3N_4 nanosheet. The stability of the α-S is largely enhanced by the heterojunction construction. The excellent photocatalytic ability and stability of α-S@C_3N_4 composite demonstrate a great potential for its usage in environmental remediation technology as a high efficient photocatalyst.

The core-shell heterojunctions of α-S@C_3N_4 are successfully fabricated via self-assemble process by electrostatic force. The enhancement of photocatalytic ability of α-S@C_3N_4 composite could be attributed to the efficient photogenerated holes and electrons separation by the heterojunction, which has excellent charge transfer ability arisen by ultra-thin C_3N_4 nanosheet. a The stability of the α-S is largely enhanced by the heterojunction construction. The excellent photocatalytic ability and stability of α-S@C_3N_4 composite demonstrate a great potential for its usage in environmental remediation technology as a high efficient photocatalyst.

Acknowledgement

This work was supported by the National Science Fund China (project no. 21107007) and Cultivation Program for Excellent Talents of Science and Technology Department of Liaoning Province (No. 2014026009).

References

1. L. F. Yin, J. F. Niu, Z. Y. She and J. Chen, *Environ. Sci. Technol.* 2010, **44,** 5581-5586.

2. X. D. Zhang, W. M. Liao, W. Wu, D. J. Zheng, Y. S. Zhou, B. L. Xue, W. Liu, Z. Q. Lin and Y. L. Deng, *J. Mater. Chem. A*, 2014, **2**, 11035-11039.

3. M. D. Ye, M. Y. Wang, D. J. Zheng, N. Zhang, C. J. Lin and Z. Q. Lin, *Nanoscale* 2014, **6**, 3576-3584.

4. Z. H. Kang, C. H. A. Tsang, N. B. Wong, Z. D. Zhang and S. T. Lee, 2007, **129**, 12090-12091.

5. Y. D. Chiou and Y. J. Hsu, *Appl. Catal. B: Environ.* 2011, **105**, 211-219.

6. F. Wang, W. K. H. Ng, J. C. Yu, H. J. Zhu, C. H. Li, L. Zhang, Z. F. Liu and Q. Li, *Appl. Catal. B: Environ.* 2012, **111**, 409-414.

7. G. Liu, P. Niu, L. C. Yin and H. M. Cheng, *J. Am. Chem. Soc.* 2012, **134**, 9070-9073.

8. W. J. Wang, J. C. Yu, D. H. Xia, P. K. Wong and Y. C. Li, *Environ. Sci. Technol.* 2013, **47**, 8724-8732.

9. W. C. Peng and X. Y. Li, *Nano Res.* 2013, 6, 286-292.

10. M. R. Hoffmann, S. T. Martin, W. Choi and D. W. Bahemann, *Chem. Rev.* 1995, **95**, 69-96.

11. Y. D. Liu, J. Goebla and Y. D. Yin, *Chem. Soc. Rev.* 2013, **42**, 2610-2653.

12. X. J. Dai, Y. S. Luo, W. D. Zhang and S. Y. Fu, *Dalton Trans.* 2010, **39**, 3426-3432.

13. Q. Xiang, J. Yu and M. Jaroniec, *Chem. Soc. Rev.* 2012, **41,** 782-796.

14. X. F. Zhang, X. Quan, S. Chen and H. T. Yu, *Appl. Catal. B: Environ.* 2001, **105**, 237-242.

15. X. C. Wang, K. Maeda, A. Thomas, K. Takanabe, G. Xin, J. M. Carlsson, K. Domen and M. Antonietti, *Nat. Mater.* 2009**, 8**, 76-80.

16. K. Maeda, X. C. Wang, Y. Nishihara, D. L. Lu, M. Antoniett and K. Domen, *J. Phys. Chem. C* 2009, **113**, 4940-4947.

17. S. C. Yan, Z. S. Li and Z. G. Zou, *Langmuir* 2009, **25**, 10397-10401.

18. J. Xu, L. W. Zhang, R. Shi and Y. F. Zhu, *J. Mater. Chem. A* 2013, **1**, 14766-14772.

19. H. X. Zhao, H. T. Yu, X. Quan, S. Chen, H. M. Zhao and H. Wang, *RSC Adv.* 2014, **4**, 624-628.

20. S. Chu, X. M. Zheng, F. Kong, G. H. Wu, L. L. Luo, Y. Guo, H. L. Liu, Y. Wang, H. X. Yu and Z. G. Zou. *Mater. Chem. Physics* 2011, **129**, 1184-1188.

21. S. Chu, Y. Wang, Y. Guo, J. Y. Feng, C. C. Wang, W. J. Luo, X. X. Fan and Z. G. Zou, *ACS Catal.* 2013, **3**, 912-919.

22. Y. J. Zhang, A. Thomas, M. Antonietti and X. C. Wang, *J. Am. Chem. Soc.* 2009, **131**, 50-51.

23. K. Schwinghammer, B. Tuffy, M. B. Mesch, E. Wirnhie, C. Martineau, F. Taulelle, W. Schnick, J. Senker and B. V. Lotsch, *Angew. Chem. Int. Ed.* 2013, **52**, 2435-2439.

24. J. Zhang, M. Zhang, R. Q. Sun and X. Wang, *Angew. Chem. Int. Ed.* 2012, **51**, 10145-10149.

25. X. D. Zhang, X. Xie, H. Wang, J. J. Zhang, B. C. Pan and Y. Xie, *J. Am. Chem. Soc.* 2013, **135**, 18-21.

26. H. Wang, X. Quan, H. T. Yu and S. Chen, *Carbon* 2008, **46**, 1126-1132.